Science Advances
AAAS

Supplementary Materials for

Phosphorylation of Doc2 by EphB2 modulates Munc13-mediated SNARE complex assembly and neurotransmitter release

Hong Zhang *et al.*

Corresponding author: Cong Ma, cong.ma@hust.edu.cn; Youming Lu, lym@hust.edu.cn

Sci. Adv. **10**, eadi7024 (2024)
DOI: 10.1126/sciadv.adi7024

The PDF file includes:

Other Supplementary Material for this manuscript includes the following:

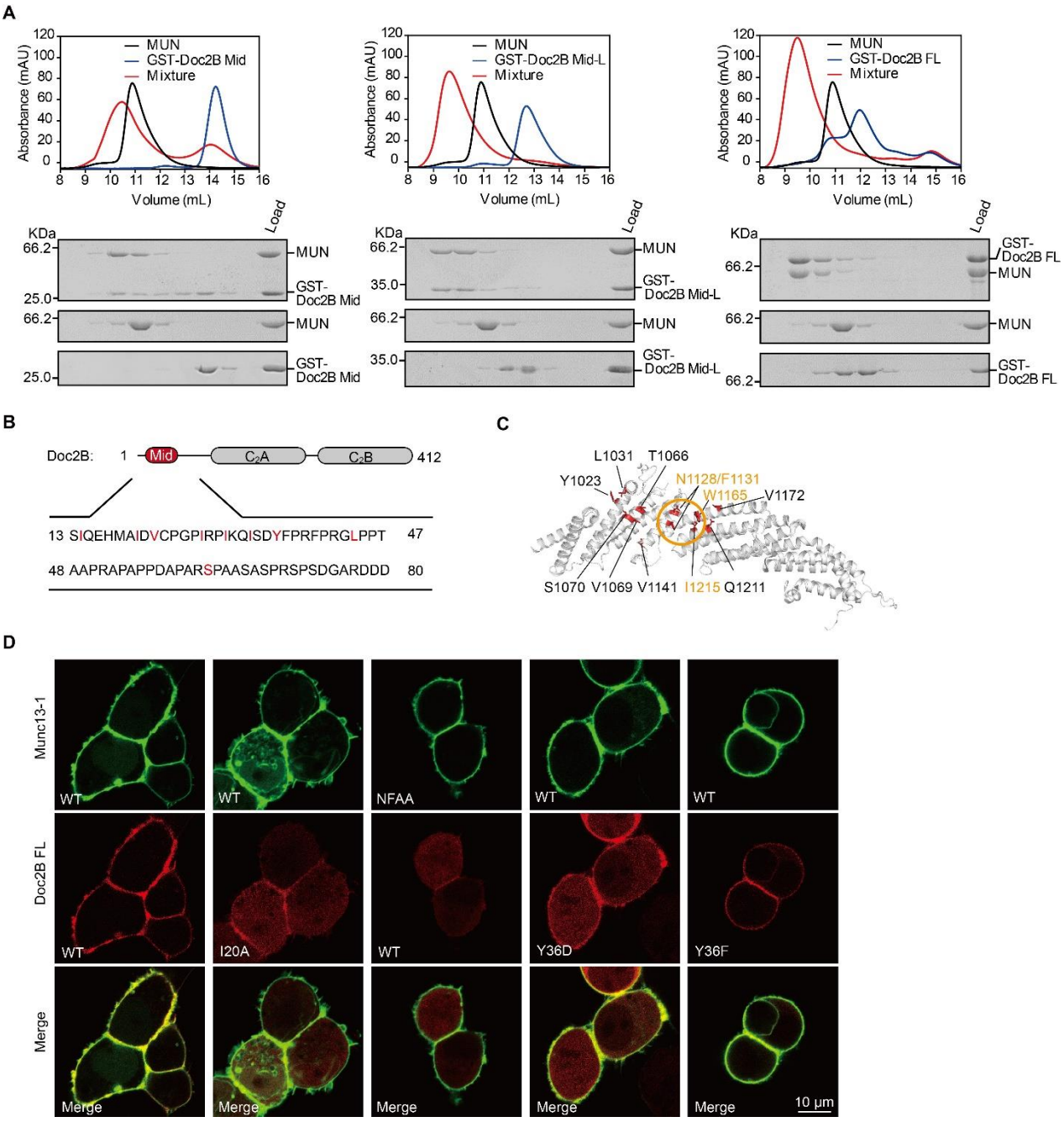

fig. S1. Doc2B Mid-L and Munc13 NF pocket mediate the Doc2B–MUN interaction
(A) Size-exclusion chromatography and SDS-PAGE showing the formation of a stable heterodimeric complex between Doc2B Mid-L (or Doc2B FL) and the MUN domain.
(B) Domain structure of Doc2B and amino-acid sequence of Doc2B Mid-L. Individual mutations of Doc2B tested in Fig. 1G are highlighted in red.
(C) Mutation sites displayed in the structure of the Munc13-1 MUN domain. Individual mutations in the MUN domain tested in Fig. 1I are highlighted in red. The residues essential for forming the NF pocket are circled and colored orange.
(D) Plasma membrane translocation of Munc13-1 (C_1C_2BMUN) and Doc2B upon PMA

stimulation in HEK293 cells. mCherry-tagged Doc2B WT or Doc2B Y36F translocates together with EGFP-tagged C_1C_2BMUN, whereas Doc2B I20A, Doc2B Y36D or C_1C_2BMUN NFAA mutation strongly impairs their co-translocation. Scale bars, 10 μm.

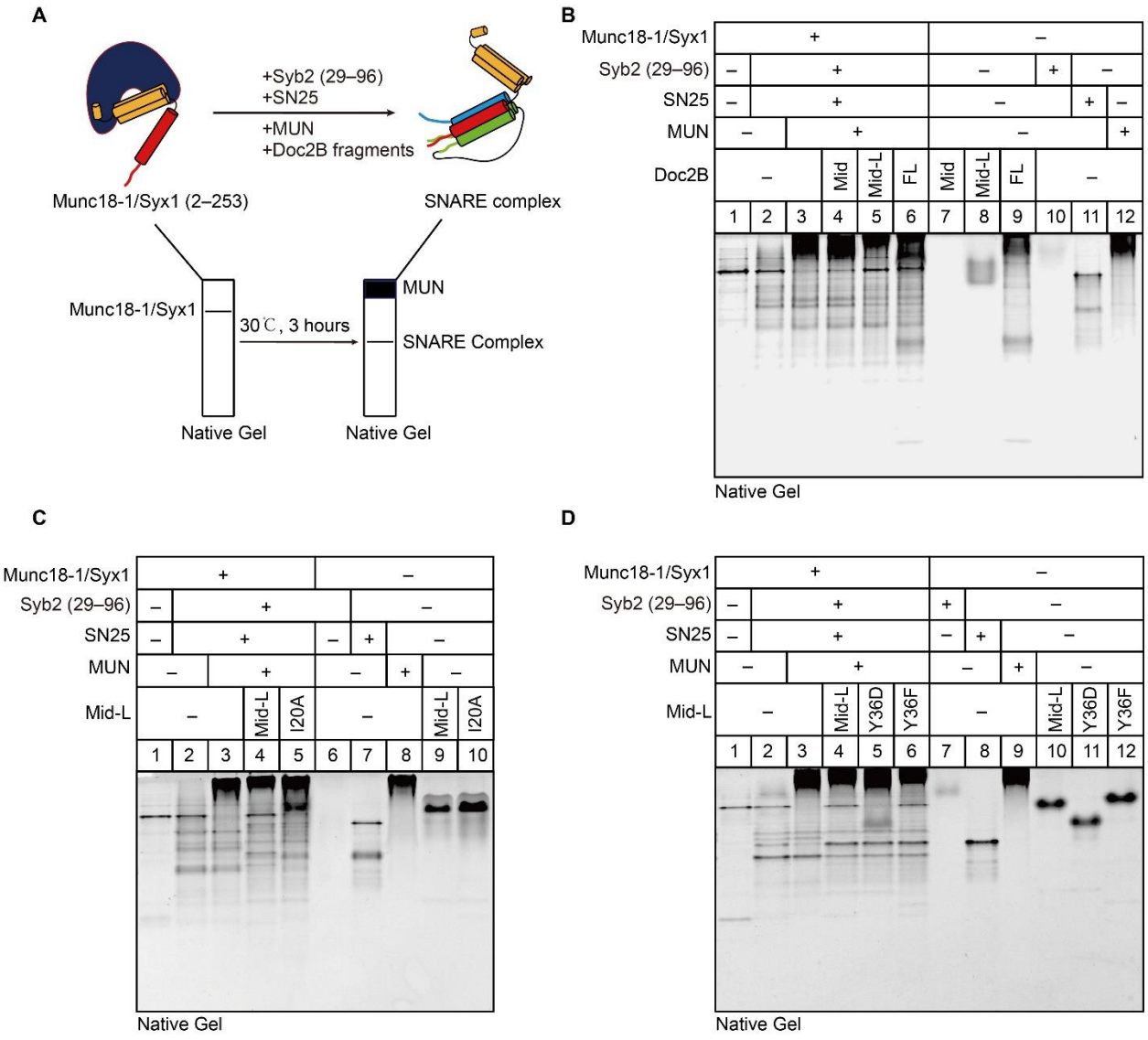

fig. S2. Doc2B Mid-L constrains MUN-catalyzed SNARE complex assembly

(A) Illustration of native-PAGE experiment for monitoring MUN-catalyzed SNARE complex assembly starting from the Munc18-1/Syx1 (2–253) complex in the presence of Syb2 (29–96) and SN25. The Munc18-1/Syx1 (2–253) complex displays a sharp band at the top of the gel; upon the addition of the MUN domain, SN25, and Syb2, this band disappears indicating the transition of the Munc18-1/Syx1 complex to the SNARE complex.

(B–D) Inhibition effects of Doc2B Mid, Doc2B Mid-L or Doc2B FL (B), Mid-L or Mid-L I20A (C), Mid-L Y36D or Mid-L Y36F (D) on MUN-catalyzed SNARE complex assembly starting from the Munc18-1/Syx1 complex detected by native-PAGE experiments.

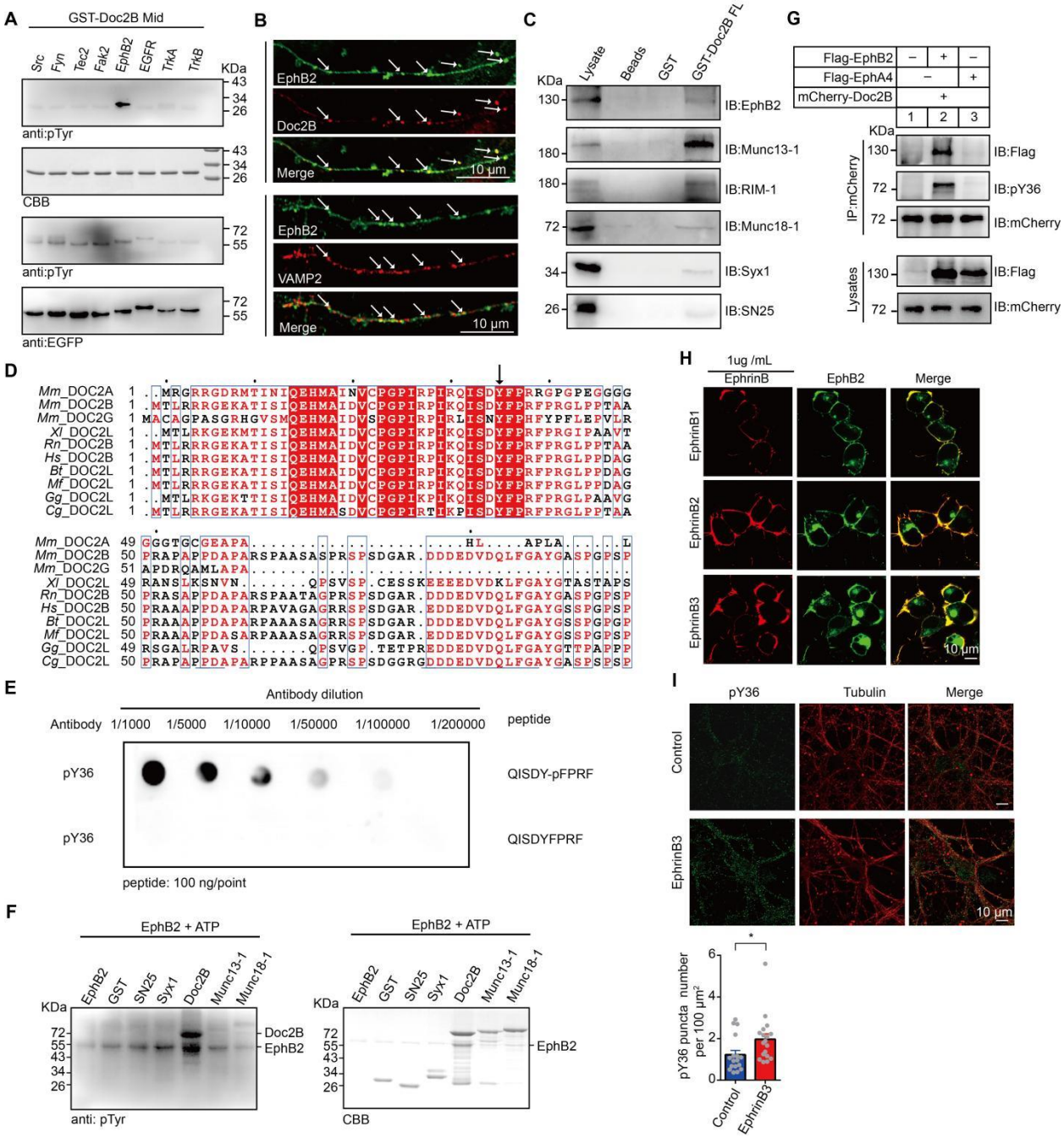

fig. S3. EphB2 specifically phosphorylates Doc2B

(A) Screening of potential tyrosine kinase that phosphorylates Doc2B. Purified tyrosine kinases from HEK293 cells were incubated with GST-Doc2B Mid in the presence of ATP, followed by western blot analysis of the indicated proteins.

(B) Endogenous EphB2 (green) and Doc2B (red) or VAMP2 (red) staining in cultured mouse hippocampus neurons. Arrows indicate EphB2/Doc2B or EphB2/VAMP2 colocalization. Scale bars, 10 μm.

(C) Association of Doc2B with presynaptic active zone proteins. GST-Doc2B FL was incubated with mouse brain homogenate lysates for GST pull-down experiments, followed by western blot

analysis of the indicated proteins.
(D) Alignment of N-terminal amino-acid sequence of mouse Doc2 isoforms across different species. The arrow indicates that the tyrosine residue (Y36) is conserved in Doc2 family proteins. *Mm*: *Mus musculus*; *XI*: *Xenopus laevis*; *Rn*: *Rattus norvegicus*; *Hs*: *Homo sapiens*; *Bt*: *Bos taur*us; *Mf*: *Macaca fascicularis*; *Gg*: *Gallus gallus*; *Cg: Cricetulus griseus*.
(E) Dot blot analysis of the phosphorylation state-specific pY36 antibody.
(F) In vitro phosphorylation assay using purified sumo-tagged EphB2 kinase domain and SN25 FL, Syx1 (2–253), GST-Doc2B FL, GST-MUN, or GST-Munc18-1 in the presence of ATP.
(G) Western blot analysis of Doc2B phosphorylation following transfection of various combinations of plasmids containing Flag-tagged EphB2, EphA4, and/or mCherry-tagged Doc2B in HEK293 cells.
(H) Immunostaining analysis of EphB2–EphrinB interaction. Preclustered EphrinB (1 μg/mL) were applied to EGFP-EphB2 expressed HEK293 cells for 30 min, followed by immunostaining analysis of EphrinB. Scale bars, 10 μm.
(I) Immunofluorescence analysis of Doc2 phosphorylation in the cultured mouse cortex neurons. Representative confocal images showing that cultured neurons exhibited low pY36 labeling under basal conditions (top); upon EphrinB3 stimulation, pY36 immunolabeling markedly increased (bottom). Statistical significance and *P* values were determined by Student's t test (**P* < 0.05).

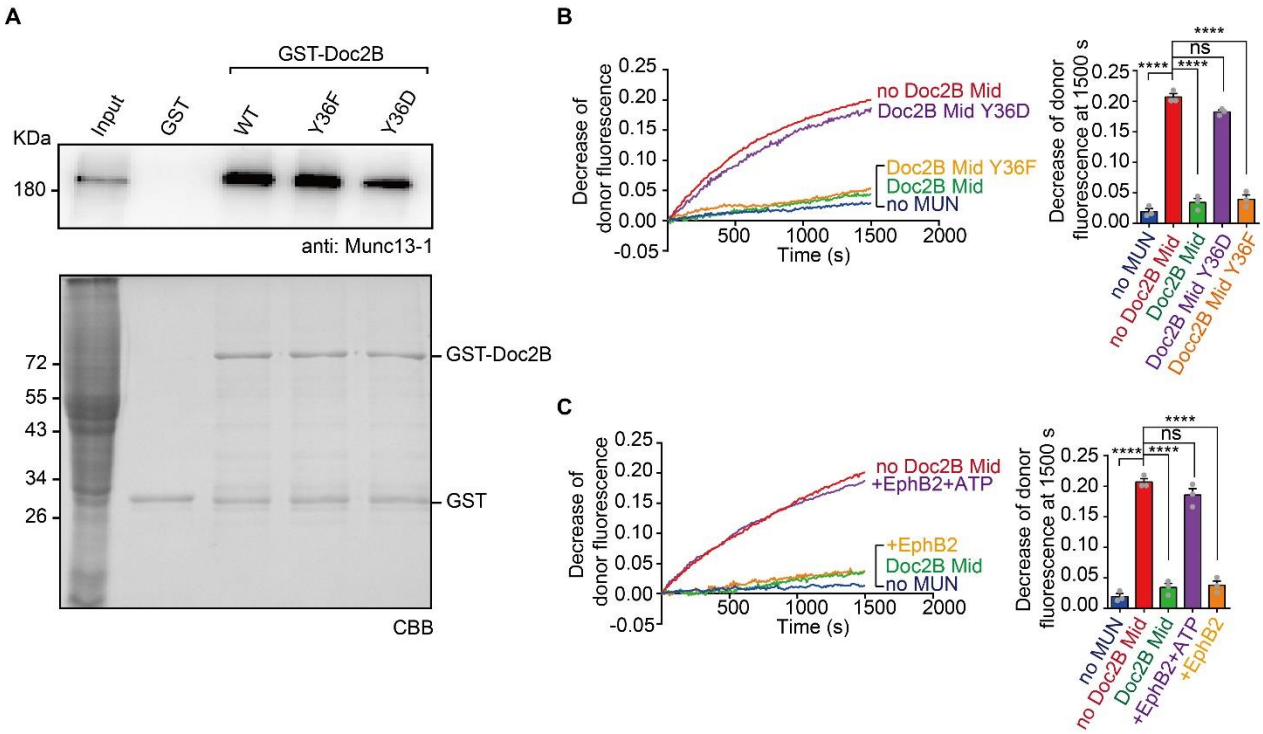

fig. S4. Phosphorylation of Doc2B Mid significantly reduces its inhibitory effect on Munc13
(A) Binding of Doc2B and its mutants with Munc13-1 FL. GST-Doc2B FL or its variant fragments was incubated with mouse brain homogenate lysates, followed by immunoblotting with anti-Munc13-1.
(B and C) MUN-catalyzed SNARE complex assembly by addition of Doc2B Mid, Doc2B Mid Y36D, or Doc2B Mid Y36F, respectively (B), addition of Doc2B Mid and EphB2 mixture in the presence or absence of ATP (C). Decrease of donor fluorescence at 1500 s is shown in the column at the right of the chart.
Data are presented as the mean ± SEM (n = 3). Statistical significance and *P* values are determined by one-way ANOVA with Dunnett's multiple comparison test (****$P < 0.0001$).

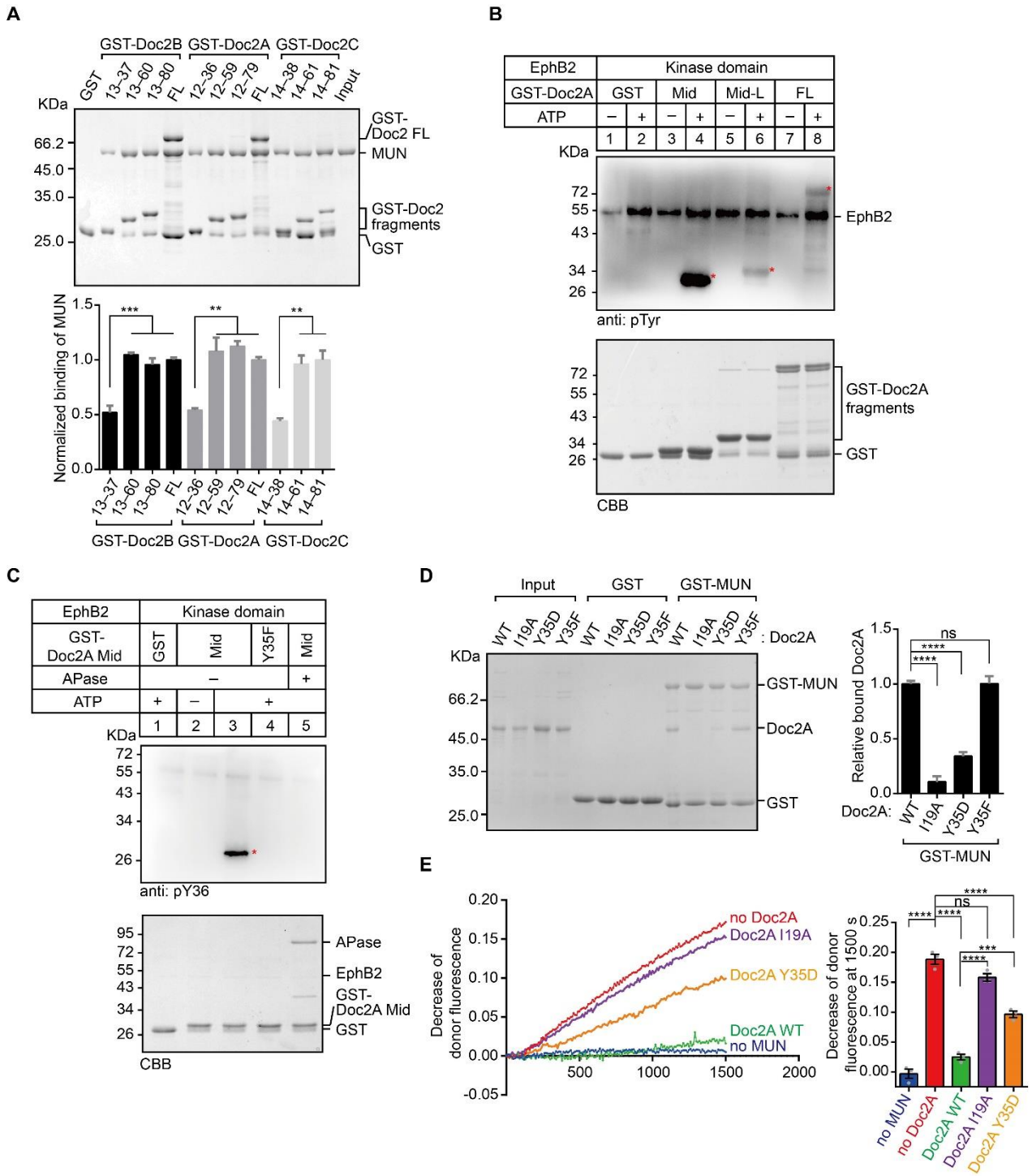

fig. S5. Doc2B phosphorylation is conserved in Doc2 family proteins

(A) Binding of the MUN domain to GST-Doc2 fragments measured by GST pull-down experiments and quantification of the binding.

(B) In vitro phosphorylation assay using purified sumo-tagged EphB2 kinase domain and GST-tagged Doc2A fragments in the presence or absence of ATP. Protein samples were resolved on SDS-PAGE and stained with CBB (bottom), and Doc2A phosphorylation was detected by

immunoblotting with anti-pTyr (top). Asterisks show bands of GST-Doc2A Mid (12–36), Mid-L (12–79), and FL, respectively.
(C) In vitro phosphorylation assay using purified sumo-tagged EphB2 kinase domain and GST-tagged Doc2A Mid or Y35F in the presence or absence of ATP and APase. Protein samples were resolved on SDS-PAGE and stained with CBB (bottom), and Doc2A phosphorylation was detected by immunoblotting with anti-pY36 antibody (top). Asterisk shows band of GST-Doc2A Mid.
(D) Binding of Doc2A FL or its variant mutations to GST-MUN measured by GST pull-down experiments and quantification of the binding.
(E) MUN-catalyzed SNARE complex assembly by addition of Doc2A WT, I19A, Y35D, or Y35F respectively. Decrease of donor fluorescence at 1500 s is shown in the column at the right of the chart.
Data are presented as the mean ± SEM (n = 3). Statistical significance and *P* values were determined by one-way ANOVA with Tukey's multiple comparisons test. ***P* < 0.01; ****P* < 0.001; *****P* < 0.0001; ns, not significant.

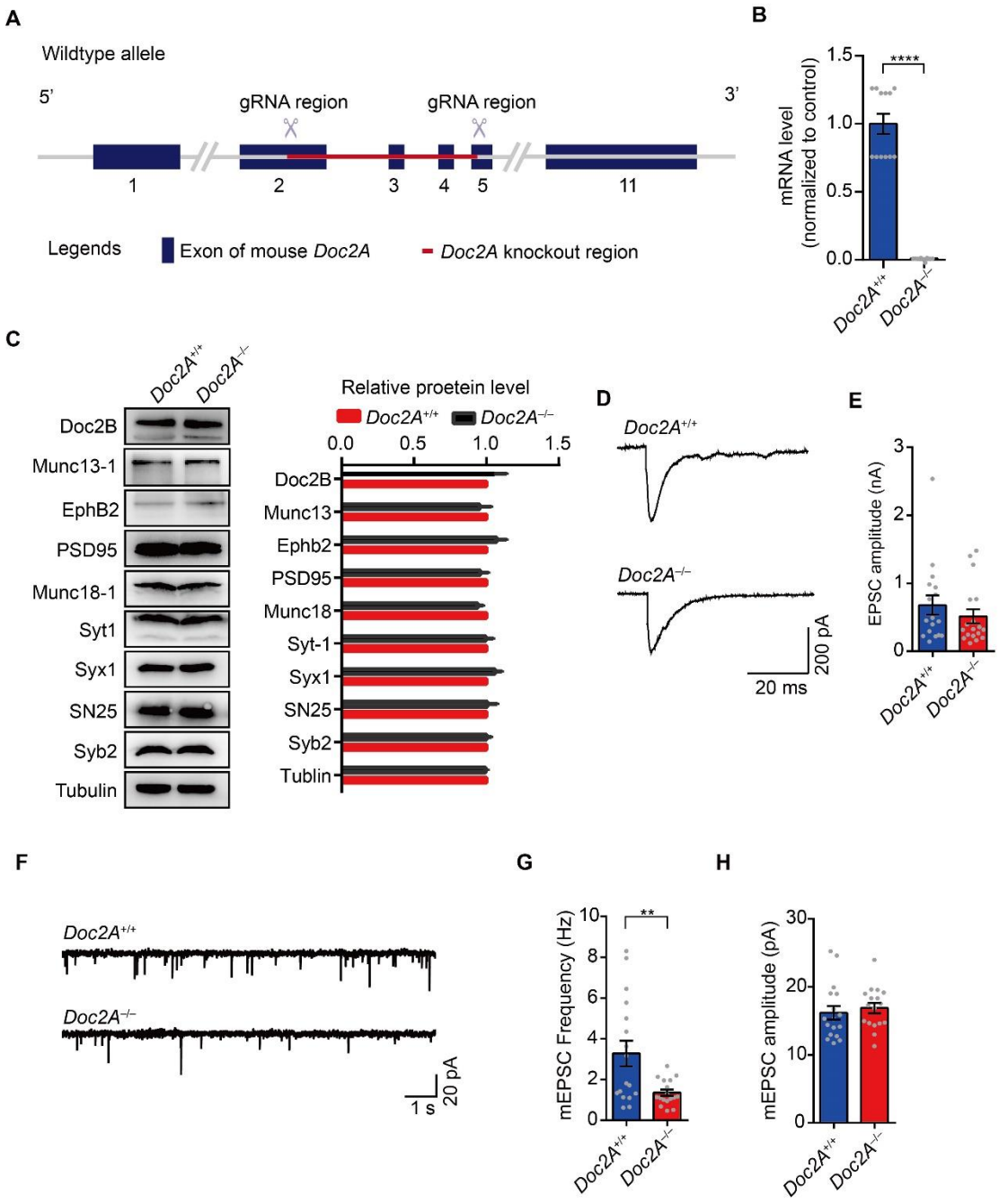

fig. S6. Doc2A deletion impairs spontaneous neurotransmitter release

(A) Generation of *Doc2A*$^{-/-}$ mouse model (C57BL/6J) by CRISPR/Cas-mediated genome engineering. 11 exons of *Doc2A* gene were identified, with the ATG start codon located in exon 2 and the TGA stop codon in exon 11. Exon 2–5 were selected as target site.

(B) Expression of Doc2A detected by qRT-PCR.

(C) Expression level of other proteins implicated in synaptic transmission detected by western blot analysis in whole mouse brain homogenate lysates.

(D and E) Representative traces (D) and summary graphs of the amplitude of evoked EPSC (E) recorded from *Doc2A*$^{+/+}$ (n = 17) and *Doc2A*$^{-/-}$ (n = 18) neurons.

(F–H) Representative traces (F), summary graphs of normalized frequency (G), and normalized amplitude (H) of mEPSC recorded from *Doc2A*$^{+/+}$ (n = 17) and *Doc2A*$^{-/-}$ (n = 17) neurons. Data are presented as the mean ± SEM. Statistical significance and *P* values were determined by Student's t test (***P* < 0.01; *****P* < 0.0001).

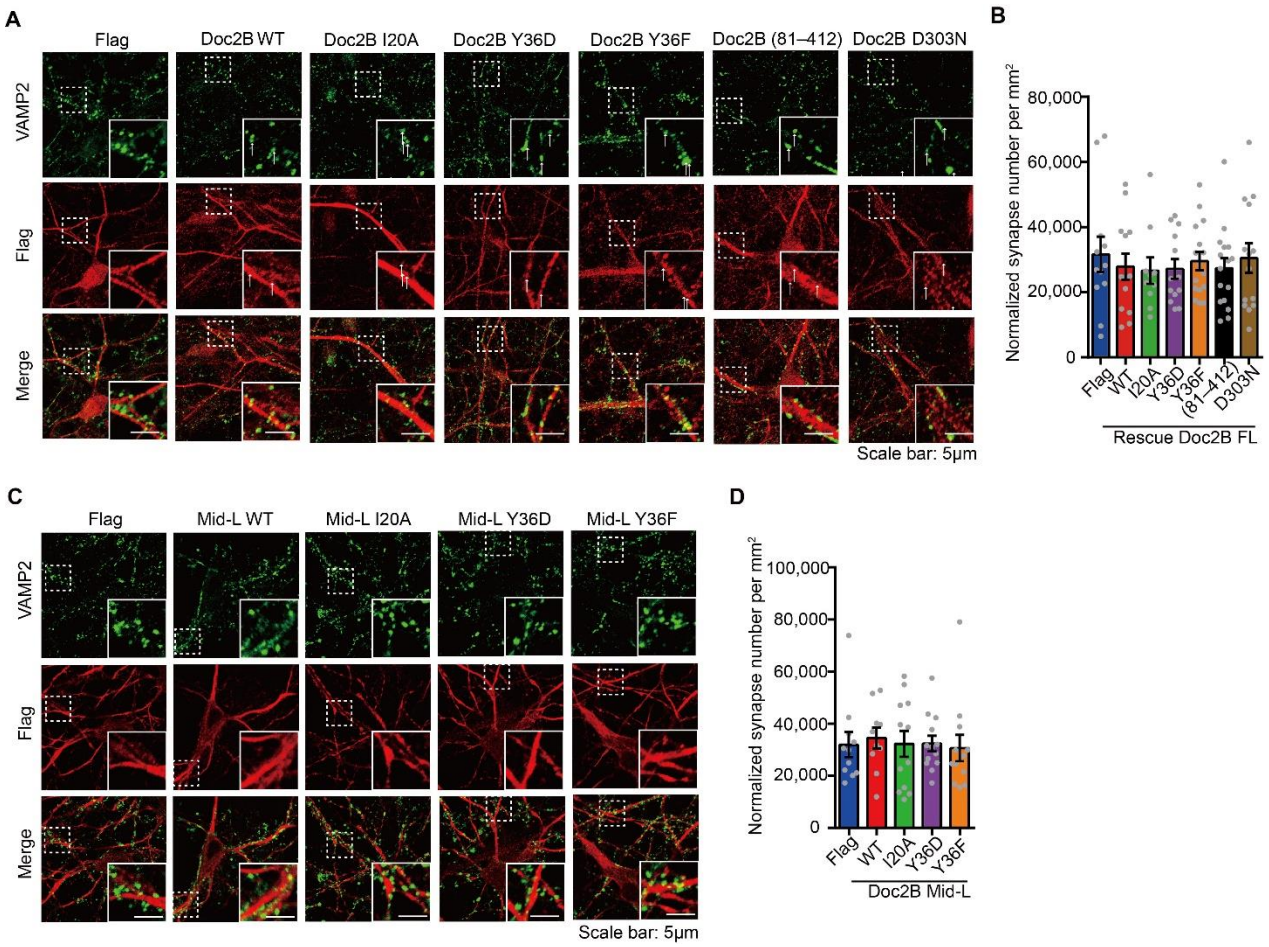

fig. S7. Lentiviral expression and localization of all variants of Doc2B

(A and B) Representative images (A) and summary graphs of synapses number (B) in cultured *Doc2A*$^{-/-}$ cortical neurons infected with control lentivirus (Flag) or with Doc2B WT, or mutants (I20A, Y36D, Y36F, 81−412, D303N). Neurons were fixed and then labeled with VAMP2 (to mark synapses, green) and Flag (to mark Doc2B, red) antibodies. Scale bar, 5 µm.

(C and D) Representative images (C) and summary graphs of synapses number (D) in cultured WT cortical neurons overexpressing control lentivirus (Flag) or with Mid-L, or mutants (I20A, Y36D, Y36F). Scale bar, 5 µm.

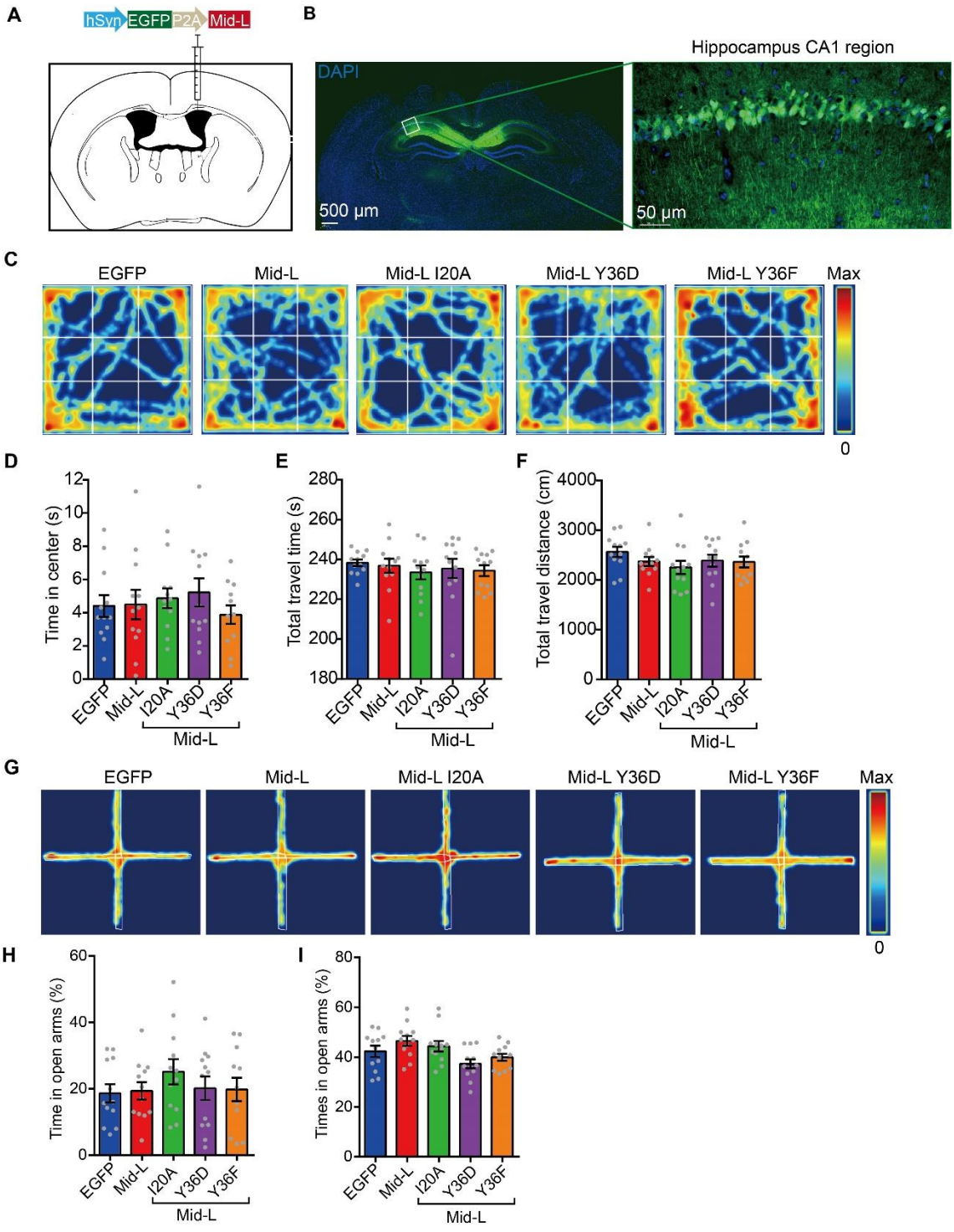

fig. S8. Disruption of the interplay between Doc2 and Munc13 has no effect on locomotor activity and anxiety

(A) The diagram of rAAV1/2 vector (top) for expression of Doc2B Mid-L and the stereotactic injection experiment (bottom) with AAV containing Doc2B Mid-L bilaterally injection into lateral ventricles.

(B) A representative fluorescence image of the virus-infected slice (left) and the expression of Doc2B Mid-L in hippocampus CA1 region (right). Nuclear DNA was labeled with DAPI (blue).
(C–F) The open field test. Representative hotspots of path tracings are shown in (C). Total time (seconds) spent in the center arena (D), total travel time (seconds) (E), and total travel distance (centimeter) (F) in the open field test were analyzed.
(G–I) The elevated plus maze test. Representative hotspots of path tracings are shown in (G). The percentage of time (H) or times (I) in open arms were analyzed.
Data are presented as the mean ± SEM (n = 12 mice per group). Statistical significance and *P* values were determined by one-way ANOVA with Dunnett's multiple comparison test.

Munc13-1	Doc2B	N (sites)	K_d (μM)	ΔH (kcal/mol)	-TΔS (kcal/mol)	ΔG (kcal/mol)
MUN	1−37	0.95 ± 0.01	1.77 ± 0.16	-5.63 ± 0.11	-2.22	-7.85
	13−37	0.96 ± 0.01	1.47 ± 0.18	-6.06 ± 0.15	-1.90	-7.96
	13−60	0.97 ± 0.01	0.23 ± 0.03	-7.63 ± 0.10	-1.43	-9.06
	13−80	1.00 ± 0.01	0.16 ± 0.02	-7.79 ± 0.09	-1.49	-9.28
	13−120	0.89 ± 0.01	0.19 ± 0.06	-7.51 ± 0.26	-1.66	-9.17
	38−80	not detectable				
	1−412	0.96 ± 0.01	0.12 ± 0.02	-8.04 ± 0.09	-1.39	-9.44
	I20A	not detectable				
	Y36D	1.16 ± 0.01	1.21 ± 0.15	-6.35 ± 0.16	-1.73	-8.07
	Y36F	1.06 ± 0.01	0.22 ± 0.02	-7.67 ± 0.27	-1.40	-9.08

Table S1. Binding of all variants of Doc2B to MUN measured by ITC-based experiments.

Other Supplementary Materials for this manuscript include the following:

Data S1. Summary of the source data obtained from in vitro experiments, encompassing Fig 1, Fig 2, and Fig 4.

Data S2. Summary of the source data obtained from electrophysiological experiments, encompassing Fig 5 and Fig 6.